WILEY-VCH

FULL PAPER

Design, Syntheses, and Structure of Copper Dithione Complexes: Redox Dependent Charge Transfer

Kyle J. Colston,[a] Dr. Sara A. Dille,[a] Dr. Benjamin Mogesa,[b] Dr. Andrei V. Astashkin,[c] Dr. Jacilynn A. Brant,[d] Dr. Matthias Zeller,[e] and Dr. Partha Basu[a]*

[a]Department of Chemistry and Chemical Biology, Indiana University-Purdue University Indianapolis, 402 N. Blackford Street, Indianapolis, IN 46202.

[b]Department of Chemistry and Biochemistry, Duquesne University, 600 Forbes Avenue, Pittsburgh, PA 15282.

[c]Department of Chemistry and Biochemistry, University of Arizona, Tucson, AZ 85721

[d]Aerospace Systems Directorate, The Air Force Research Laboratory, 1950 Fifth Street, Building 18, Wright-Patterson Air Force Base, Ohio 45433

[e]Department of Chemistry, Purdue University, 560 Oval Drive, West Lafayette, IN 47907

Emails: basup@iupui.edu

Twitter:@ChemIUPUI

Abstract: Redox-active ligands impart versatility in transition metal complexes, which are attractive for photosensitizers, dye sensitized solar cells, photothermal therapy, etc. Dithiolene (Dt) ligands can transition between fully reduced and fully oxidized states. Herein, we report the syntheses, characterization, crystal structures and electronic properties of four $[Cu(R_2Dt^0)_2]^{+/2+}$ (R = Me, ^{i}Pr) complexes, $[Cu(^iPr_2Dt^0)_2][PF_6]$ (**1a**), $[Cu(^iPr_2Dt^0)_2][PF_6]_2$ (**1b**), and $[Cu(Me_2Dt^0)_2][PF_6]$ (**2a**), $[Cu(Me_2Dt^0)_2][PF_6]_2$ (**2b**), where $^iPr_2Dt^0$ = *N,N'*-diisopropyl-1,2-piperazine dithione and Me_2Dt^0 = *N,N'*-dimethyl-1,2-piperazine dithione. In addition, the molecular structure of $[Cu(^iPr_2Dt^0)_2][BF_4]_2$(**1c**) is also reported. Complexes **1a** and **2a** crystallized in the triclinic, $P\bar{1}$ space group, and **1c** crystallized in the monoclinic crystal system, space group $C_{2/c}$. The single crystal X-ray diffraction measurements show that the Cu(I) complexes have a distorted tetrahedral geometry, whereas the Cu(II) complex exhibits a true square planar geometry. Cu(I) complexes exhibit a low energy charge transfer band (450-650 nm), which are not observed in Cu(II) complexes. Electrochemical studies of these complexes show both ligand- and metal-based redox couples.

Introduction

Understanding the process of electron transfer into and out of a redox core is of fundamental importance in materials and biological chemistry. Transition metal complexes can exhibit multiple metal-centered oxidation states and adopt different geometries. Such versatility makes transition metal complexes of interest for materials applications. This variability can be extended by the coordination of redox active ligands, such as dithiolene (Dt), to redox active metal centers. Such properties increase the number of accessible redox states in a molecular system. The ability to add or remove electrons in transition metal dithiolene complexes is determined by the geometry of the complex and redox potentials of both the transition metal and the ligand. Conceptually, the two extreme forms of dithiolene ligands[1] are the fully reduced 1,2-ene-dithiolate(2-) state (Dt^{2-}) and the fully oxidized dithione state (Dt^0). The ability to transition between the different oxidation states allows dithiolene complexes to generate short-lived electronic excited-states, where one ligand is reduced and the other is oxidized in a single-electron ligand to ligand charge transfer (LLCT) process.[2] Intramolecular LLCT and mixed-metal LLCT (MMLLCT) transitions make dithiolene metal complexes exceptionally potent in charge transfer processes. [3]

Access to these intricate redox states has led to the development of transition metal complexes containing redox-active dithiolene ligands as potential conducting[4] and magnetic[4a, c, e, k, 5] materials. In addition, the optical properties are of interest in developing near-infrared (NIR) dyes and nonlinear optical materials.[6] Pioneering research on platinum and nickel charge-transfer photosensitizers[7] highlights the importance of redox-active ligands in photoexcited materials. Platinum and nickel dithiolene complexes also show promise as NIR dyes with possible applications in dye sensitized solar cells[8] and photothermal therapy.[9] The ligands in this work are based on the fully oxidized dithione form of the dithiolene ligand that contains a C(=S)-C(=S) unit. and the dithione unit coordinates to the metal in a charge neutral state.[10] Interconversion between redox states that facilitate charge transfer has been a driving force behind the development of copper ene-1,2-dithiolate(2-) complexes.[11] The electronic excitation energies and redox potentials in these systems can be tuned through chemical modification of the dithiolene ligand,[11b] but such modifications may impact complex stability.[11c]

Transition metal complexes of dithione ligands exhibit electron delocalization across the metal and non-innocent ligands, forming π-orbital donor-acceptor systems.[12] [13] Cu(I) complexes adopt a tetrahedral geometry, whereas Cu(II) complexes prefer a square-planar geometry.[14] Changing the geometry between the two oxidation states results in significant differences in electronic structure that can be attributed to a geometry-based gating of copper-dithiolene orbital mixing. Upon oxidation of the metal center from Cu(I) to Cu(II), there is a decrease in copper and sulfur orbital covalency as the square planar geometry makes LLCT more favorable. Thorough characterization of systems with

This is the author's manuscript of the article published in final edited form as:

Colston, K. J., Dille, S. A., Mogesa, B., Astashkin, A. V., Brant, J. A., Zeller, M., & Basu, P. (2019). Design, Syntheses, and Structure of Copper Dithione Complexes: Redox Dependent Charge Transfer. European Journal of Inorganic Chemistry. https://doi.org/10.1002/ejic.201901222

geometry-dependent charge transfer processes is required to produce an accurate model of the donor-acceptor charge transfer systems. In this manuscript, we focus on homoleptic Cu(I/II) complexes of dithione ligands and report their synthesis and characterization. Target complexes (Chart 1) are prepared from copper salts with two closely related dithione ligands, *N,N*-dimethyl piperazine 2,3-dithione (Me_2Dt^0) and *N,N*-diisopropyl piperazine 2,3-dithione ($^iPr_2Dt^0$). [15] We report the electrochemical, spectral, and magnetic properties of these complexes, as well as their molecular and electronic structures.

Chart 1

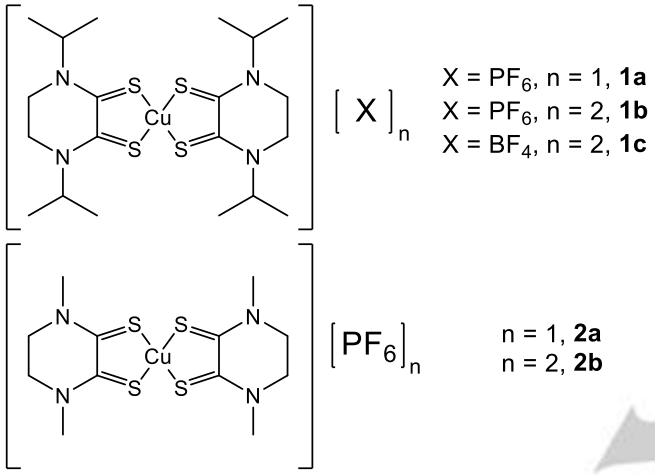

Results and Discussion

Synthesis and characterization

Complexes **1a** and **2a** were isolated in 32% and 48 % yields, respectively. The modest yields were due to the repeated washing to remove excess $NaPF_6$ to provide analytically pure materials. Complexes **1b** and **2b** were synthesized from $CuCl_2{\cdot}2H_2O$ salt with two equivalents of dithione ligand with 94% and 62% yields, respectively. All complexes are soluble in polar solvents such as acetonitrile, methanol, ethanol or THF. The Cu(I) complexes are purple in solution, while the Cu(II) complexes are green. In air, acetonitrile solutions of Cu(I) complexes are stable for days at standard conditions, while Cu(II) complexes reduce to Cu(I) over the course of hours. In the solid state, all complexes are stable in air. The observed molar conductivities of **1a** and **2a** suggest a 1:1 electrolyte ratio , while **1b** and **2b**, show a 1:2 electrolyte ratio, as expected.[16]

The ^{13}C NMR spectra of **1a** and **2a** exhibit a peak at 183 ppm and 182 ppm, respectively, due to the presence of C=S moieties. The corresponding resonances from the free dithione ligands $^iPr_2Dt^0$ and Me_2Dt^0 appear at 181 ppm and 180 ppm, respectively. Therefore, there is a small (~2 ppm) downfield shift due to metal coordination. The ^{13}C NMR data are consistent with the coordinated fully oxidized dithione ligand. The solid-state IR spectra of Cu(I) complexes, **1a** and **2a**, show C=S stretching frequency at 1,352 cm^{-1} and at 1,356 cm^{-1}, respectively. For the Cu(II) complexes, the frequency was 1,364 cm^{-1}. The ~8 cm^{-1} difference between the observed frequencies between the Cu(I) and Cu(II) complexes is due to the change in the oxidation state of the metal. In the free ligand, the C=S stretching frequency is observed at 1,335 cm^{-1}. Thus, there is a ~19 cm^{-1} shift in the C=S stretching frequency upon coordination. IR and NMR spectroscopic data supports that the ligands remain fully oxidized in both solution and solid states.

Molecular structures

The molecular structures of **1a**, **2a** and **1c** have been determined by X-ray crystallography. All single crystals were grown by slow diffusion of an acetonitrile solution of the target complex into diethyl ether. Crystallographic data are listed in Table 1. Green needle shaped crystals were obtained for all crystals. Attempts to grow single crystals of **1b** and **2b** resulted in the reduction of the Cu(II) center even under inert atmosphere conditions. Thermal ellipsoid plots for **1a** and **2a** are shown in Figure 1 and the thermal ellipsoid plot for **1c** is shown in Figure 2. Select bond lengths and angles are given in Tables 2 and 3. **1a** and **2a** both crystallized in the triclinic crystal system ($P\bar{1}$ space group), with Z = 4 and 2, respectively. Complex **1c** crystallized in the monoclinic crystal system and the $C_{2/c}$ space group (Z = 4). Complexes **1a** and **2a** exhibit a distorted tetrahedral geometry while complex **1c** exhibits a square planar geometry. Select bond lengths for **1a** and **1c** are shown in Table 2., and bond lengths of **2a** are given in the supporting information (Table S1). Crystal density was calculated for each structure and showed that **1a** and **1c** were almost identical in density, while **2a** was calculated to be denser than **1a** by 0.36 g/cm^3 (Table S2). The crystal lattice of **2a** is also more ordered than for both **1a** and **1c** (Figure S1).

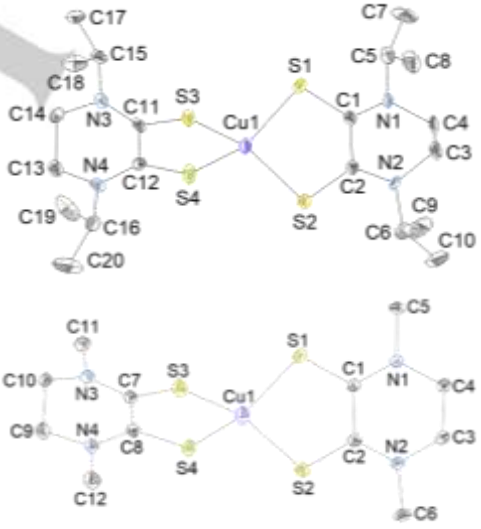

Figure 1. Thermal ellipsoid plots (30%) for **1a** (top) and **2a** (bottom). Hydrogen atoms and anions have been omitted for clarity.

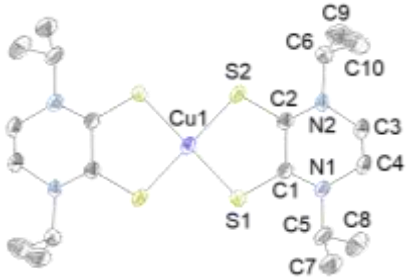

Figure 2. Thermal ellipsoid plot of **1c** (30%) presented as described in Figure 1.

10.1002/ejic.201901222

FULL PAPER

Table 1. Crystal data and structure refinement for $[Cu(^{i}Pr_2Dt^{0})_2][PF_6]$ (**1a**) $[Cu(Me_2Dt^{0})_2][PF_6]$ (**2a**), and $[Cu(^{i}Pr_2Dt^{0})_2][BF_4]_2$ (**1c**)

	1a	**2a**	**1c**
Empirical formula	$C_{20}H_{36}CuF_6N_4PS_4$	$C_{12}H_{20}CuF_6N_4PS_4$	$C_{20}H_{36}B_2CuF_8N_4S_4 . C_2H_3N$
Formula weight	669.28	557.07	738.98
Temperature	296 K	150 K	296 K
Crystal system	Triclinic	Triclinic	Monoclinic
Space Group	$P\bar{1}$	$P\bar{1}$	C2/c
a/Å	12.863(4)	6.7651(3)	22.7593(4)
b/Å	13.49 2(4)	12.0158(5)	14.7561(3)
c/Å	19.16 (4)	12.8668(5)	11.7167(2)
c/Å	70.120 (15)	91.934(2)	90
α/°	71.199 (5)	100.207(2)	120.11(10)
β/°	89.990 (4)	97.709(2)	90
Volume/Å^3	3038.3(15)	1018.29(7)	3403.62(11)
Z	4	2	4
Radiation	MoKα	MoKα	MoKα
Crystal size/mm^3	0.21 x 0.07 x 0.09	0.6 x 0.3 x 0.1	0.20 x 0.08 x 0.07
Reflections collected	36133	6509	31562
Independent reflections	18202	6509	5729
Restraints/parameters	930/783	0/258	160/254
Goodness-of-fit on F^2	1.02	1.08	1.01
Final R	R_1 = 0.074, wR_2 = 0.225	R_1 = 0.034, wR_2 = 0.107	R_1 = 0.039, wR_2 = 0.113

Table 2. Selected bond lengths for the crystal structures of **1a** and **1c.**

$[Cu(^{i}Pr_2Dt^{0})_2][PF_6]$ (**1a**)				$[Cu(^{i}Pr_2Dt^{0})_2][PF_6]_2$ (**1c**)			
Bond length, Å		Bond angle, °		Bond length, Å		Bond angle, °	
Cu1- S1	2.291(4)	S3-Cu1-S1	138.66(17)	Cu1-S1	2.2795(5)	S1-Cu-S2	89.447(18)
Cu1- S2	2.291(4)	S3-Cu1-S2	104.66(17)				
Cu1-S3	2.289(4)	S1-Cu1-S2	91.95(12)	Cu1-S2	2.2606(5)	S1-Cu-S1^{i}	180.0
Cu1-S4	2.305(3)	S3-Cu1-S4	91.43(12)				
C1- S2	1.672(11)	S1-Cu1-S4	100.42(13)	S1-C1	1.6936(16)	S1^{i}-Cu-S2^{i}	89.445(18)
C2-S1	1.702(13)	S2-Cu1-S4	138.99(16)				
C11- S3	1.705(12)	C2-S1-Cu1	100.0(4)	S2-C2	1.6880(18)	S2-Cu-S2^{i}	180.0
C12-S4	1.686(12)	C1-S2-Cu1	100.9(4)				
C1-C2	1.513(3)	C7-S3-Cu1	101.67(9)	C1-C2	1.499(3)	-	-
C1-N19	1.332(3)	C8-S4-Cu1	101.86(10)				

The observed Cu-S, C-S, and C-C bond lengths in **1a**, **2a** and **1c** suggest that the dithione ligands remain oxidized. A recent search on the Cambridge Crystallographic Data Centre (CCDC) showed records for 138 $[Cu^{II/III}(Dt^{2-})_2]^{3-/2-}$ complexes and one $[Cu^{II}(Dt^{0})_2]^{2+}$ [17] complex, $[Cu(Hdbzdto)_2][ClO_4]_2$ where Hdbzdto= *N,N'*-dibenzyldithiooxamide). The CCDC search revealed that most of the known Cu-dithiolene complexes are Cu(II) structures with several Cu(III) structures; there are no reported structures of Cu(I) dithiolene complexes.[18] The two bonds of importance for determining the oxidation state of dithiolene ligand are the C-S bonds and the C-C bonds of the dithiolene moiety. The average length for a C-S bond in the dithiolene structures was 1.73 Å (Figure S2) and the C-C bond was 1.36 Å (Figure S3) whereas the C-S bond in the dithione structure was 1.66 Å -1.67 Å and the C-C bond length was 1.49 Å. Complexes **1a**, **2a**, and **1c** have C-S bonds that are shorter than those of the dithiolene complex and are approximately the same length as in the dithione complex. The C-C bonds of **1a, 2a,** and **1c** are also longer than those in the dithiolene complexes and are approximately the same length as the C-C bond in the other dithione complex, the bond lengths are listed in Table 3.

Table 3. Comparison of average bond lengths (Å).

Complex	Cu-S	S-C	C-C	C-N
Average Ditholene	2.25(1)	1.72(3)	1.36(6)	-
$[Cu(Hdbzdto)_2][ClO_4]_2$	2.28(8)	1.67(1)	1.49(7)	1.31(6)
1a	2.29(4)	1.69(1)	1.50(8)	1.34(5)
2a	2.26(9)	1.67(6)	1.51(3)	1.32(6)
1c	2.27(5)	1.68(5)	1.50(5)	1.31(1)

The average Cu-S bond length for **1c**, is 2.27 Å, which is slightly shorter than Cu(I) complex **1a,** with the same ligand system. The Cu-S bond lengths change with the oxidation state of the metal.[19] Similar trends are also seen in dithiolene Cu(III)/Cu(II) complexes, where the Cu-S bond is longer in Cu(II) as compared to Cu(III).[20] The Cu-S bond length in **1c** is within the same range ~2.250–2.308 Å, which implies that the two dithione ligands used in this study could be equally coordinated to the metal center as their dithiolene (Dt^{2-}) counter parts. The C-N bond lengths in **1c** are similar to the reported values for $[Cu(Hdbzdto)_2][ClO_4]_2$, which are slightly shorter than the values observed for complexes **1a** and **2a.** This suggests more prominent enol character for the ligands of square planar dithione complexes. Complexes **1b** and **2b** have a similar electronic environment to the previously reported $[Cu(HDbzdto)_2][ClO_4]_2$, which corresponds to more covalent S–Cu(II) bonds for **1b** and **2b**.

Typically, Cu(I) complexes adopt a tetrahedral geometry in the first coordination sphere. Complexes **1a** and **2a** do not exhibit exact tetrahedral geometry, instead, they exhibit a distorted tetrahedral geometry. The distortion for tetrahedral complexes **1a** and **2a** can be quantified by the dihedral angle (λ) between the S-Cu-S planes, where both sulfur atoms belong to the same chelate. A perfect tetrahedral geometry is represented by λ = 90°, a near tetrahedron by λ = 80-90°, and an intermediate value by λ = 10-80°.[21]The calculated λ for **1a** and **2a** were 58.71° and 79.10°, respectively, indicating a moderate distortion from tetrahedral geometry, which is common for d^{10} systems. The distortion of a four-coordinate system can also be quantified by the parameter τ_4, introduced by Yang and coworkers defined as $\tau_4 = \frac{360^0-(\alpha+\beta)}{141^0}$ in which α and β are the two largest angles of the four-coordinate species.[22] Another index from Kubiak et al, τ_δ, allows to distinguish between a "true sawhorse" and tetrahedral geometries with addition of the term δ ($\delta = \frac{\beta}{\alpha}$).[23] Such parameters have been utilized to characterize the geometric distortions in similar Zn-dithione complexes.[15b] For both indices, a value of 0 indicates that a complex is perfectly square-planar while a value of 1 corresponds to a tetrahedral geometry. A value $\tau_\delta \approx 0.30$ is indicative of a sawhorse geometry. The distortion values for **1a**, **2a**, **1c**, and selected complexes are presented in Table 4 for comparison (a complete table of all known $[Cu^{II/III}(Dt^{2-})_2]^{3-/2-}$ complexes is included in supporting material Table S3). While complexes **1b** and **2b** were reduced to Cu(I) during crystal growth, complex **1c** is square planar in the first coordination sphere. Most previously reported complexes are square planar and have distortion values within 0.05 of **1c.**

Table 4. τ values for **1a, 2a, 1c**, and select previously reported $[Cu^{I/II}(Dt^{2-})_2]^{3-/2-}$ complexes

Complex	τ_4	τ_δ	Ref.
1a	0.58	0.58	This work
2a	0.77	0.76	This work
1c	0.00	0.00	This work
$[Cu(Hdbzdto)_2][[ClO4]_2$	0.00	0.00	[17]
$[Et_4N]_2[Cu\ (mnt)_2]$[a]	0.02	0.02	[24]
$[NO_{2b}zPy]_2[Cu(mnt)_2]$[b]	0.03	0.03	[25]
$[4,4'\text{-}H_{2b}py]_2[Cu(mnt)_2]$[c]	0.31	0.31	[26]

[a] mnt^{2-} = maleonitriledithiolate, [b] $NO_{2b}zPy$ = 1-(4'-nitrobenzyl)pyridinium), [c] 4,4'-H_{2b}py = 4,4'-bipyridine

The CCDC has records of 53 tetrahedral Cu(I) complexes coordinated to sulfur-based ligands and their distortion values are listed Table S4. The average τ_4 and τ_d values of tetrahedral Cu(I) complexes with sulfur-based ligands are calculated to be 0.84 (range 0.96-0.71) for both parameters, this value is close to that observed in **2a** (0.77).[27] The τ values (0.58) for **1a** are smaller than those of **2a** by 0.19, indicating **1a** is significantly more distorted than those reported in the CCDC database. The larger distortion in **1a** and flattening of the molecule is a consequence of incorporating bulky isopropyl substituents into the crystal lattice structure.

Magnetic properties

The magnetic susceptibility ($1/\chi_M$) of Complex **1b** exhibits paramagnetic behavior as expected, shown Figure 3, while **1a** demonstrates very slight paramagnetic behavior (Figure S4). For **1b**, the $\chi_M T$ is estimated as ~0.33 from the data in Figure 3. $\chi_M T = 1/2 \bullet S(S+1)$, so S = 0.45, which corresponds to an effective magnetic moment of 1.61 μ_B/Cu since $\mu_{Cu} = 2\sqrt{(S(S+1))}$.[28] The

μ_{Cu} is slightly lower than the spin-only magnetic moment (μ_s) of 1.73 μ_B for Cu^{2+}.

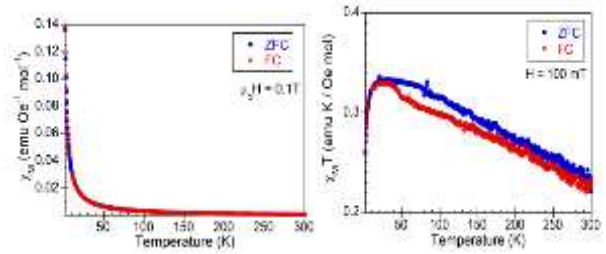

Figure 3. Magnetic properties and temperature dependence of molar magnetic susceptibility of **1b**.

Room temperature CW EPR spectra of **1b** and **2b** in acetonitrile (Figure 4a) exhibit the typical four-line structure due to the hyperfine interaction of the copper nucleus (^{63,65}Cu, I =3/2). From these spectra, the isotropic hyperfine coupling constants are found to be 7.8 mT for both complexes. The isotropic g-values are 2.055 for **1b** and 2.056 for **2b**. The EPR spectra of these complexes in frozen acetonitrile/toluene solutions recorded at 77 K (Figure 3**b**) exhibit axial anisotropy of the g-factor and the hyperfine interaction, with $g_{||} \approx 2.1$ and $A_{||} \approx 16.5$ mT for both complexes. These EPR parameters are typical for a Cu(II) ion coordinated by four sulfur atoms.[29]

The *g* values determined from the EPR spectrum of **1b** supports that the SOMO is based in the copper $d_{x^2-y^2}$ orbital. Calculating the *g* value from the electronic spectra of **1b**, **2b**, and $[Cu(Hbdzdto)_2][ClO_4]_2$[30] with the following equation, $g = g_0 \pm \frac{n\lambda}{\Delta E}$,[31] support that their low energy d-d transitions are $d_{x^2-y^2} \rightarrow d_{xz/yz}$ charge transfers. The term $\frac{n\lambda}{\Delta E}$ is the deviation from the free electron g-value (g_o), as determined from the amount of spin-orbit coupling from the magic pentagon diagram (*n*), the spin orbit coupling constant (λ), and the energy of the d-d transition *(ΔE)*.[31]

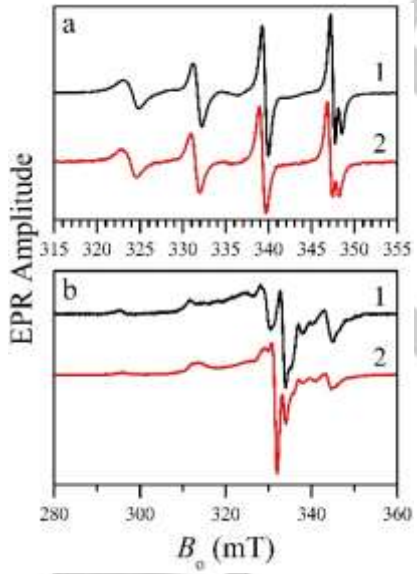

Figure 4. EPR spectra of **1b** and **2b**. Panel a: liquid CH_3CN solution at room temperature. Panel b, frozen CH_3CN/toluene (1:1 v:v) solution at 77 K. Experimental conditions for panel a: microwave (mw) frequency, 9.652 GHz; mw power, 2 mW; magnetic field modulation amplitude, 0.5 mT. Experimental conditions for panel b: mw frequency, 9.443 GHz; mw power, 0.2 mW; magnetic field modulation amplitude, 0.5 mT.

Electrochemistry

The electrochemical properties of **1a**, **1b**, **2a**, and **2b** have been investigated by cyclic voltammetry in acetonitrile. All complexes show a reversible Cu(II/I) couple at ~100 mV as shown in Figure 5. and Table 5. The Cu(II/I) couple for **1a** and **1b** are ~9 mV larger when compared to corresponding complexes **2a** and **2b**. The metal couple is ~ also 15 mV greater for complexes **1a** and **2a** when compared to **1b** and **2b**. Peak-to-peak separation (ΔE_p) for the Cu(I) complexes were higher than for the Cu(II) complexes by ~85 mV. The presence of two fully oxidized dithiolene ligands creates the potential to observe four redox couples during the reduction of the complexes; these are observed in previously reported nickel bis(dithione) complexes.[15a] None of the reported complexes in this work demonstrated reversible ligand based peaks. Instead, four poorly resolved quasi-reversible peaks between -1200 mV and -2300 mV are observed (Figures S5 and S6).

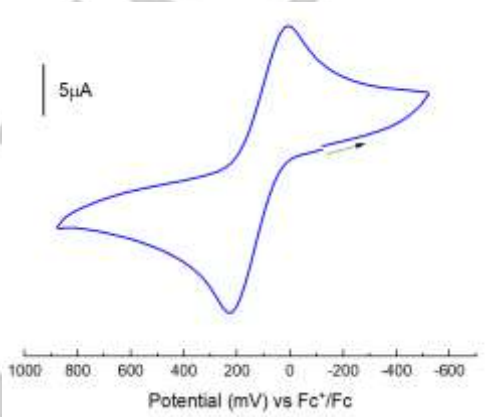

Figure 5. Cyclic voltammogram of the Cu(II/I) couple for **2a**. Scan rate, 100 mV s^{-1}; temperature 25° C; CH_3CN; Pt disk working electrode. Ag^+/Ag non-aqueous reference electrode, Pt wire auxiliary electrode, and supporting electrolyte tetrabutylammonium hexafluorophosphate (TBAP). Potentials are referenced internally with respect to the Fc^+/Fc couple.

Table 5. Room temperature Cu(II/I) redox potentials (vs Fc^+/Fc) of **1a, 2b, 2a,** and **2b** in acetonitrile.

Complex	$\Delta E_{1/2}$ (ΔE_p), mV
1a	101 (190)
1b	85 (95)
2a	110 (214)
2b	97 (140)

The differences in the redox couple for the copper center for Cu(I) and Cu(II) complexes can be attributed to changes in chemical environment, oxidation state, and coordination geometry about the copper atom. Cu(I) complexes will change from a tetrahedron to square planar upon oxidation, while the geometry in Cu(II) complexes transform to a tetrahedron when reduced. Complexes with isopropyl substituents are easier to oxidize. This is due to the superior electron donating ability of the isopropyl unit, which increases distortion observed for their primary coordination sphere. The more distorted tetrahedron experiences a milder conformational change and requires less energy. **1a** and **2a** are easier to oxidize than their Cu(II) counterparts. The smaller effective nuclear charge (Z_{eff}) of Cu(I) lowers the energy of the d-orbital manifold. Thus, the process of changing from a distorted

tetrahedron to square-planar geometry is more favored over transitioning from square planar to tetrahedron. This is reflected in the increased ΔE_p for the Cu(I) complexes as the less favored transition results in a less reversible couple.

Electronic spectra

The electronic spectra of **1a** and **1b** are shown in Figure 6 and relevant data is listed in Table 6. All complexes exhibit two intense bands between 45,000 – 30,000 cm^{-1}. In addition, the Cu(I) complexes, **1a** and **2a**, exhibit a strong electronic transition at 18,900 cm^{-1} (9,300 $M^{-1}cm^{-1}$) and 18,870 cm^{-1} (10,000 $M^{-1}cm^{-1}$), respectively. Cu(II) complexes, **1b** and **2b,** show much weaker electronic transitions at 15,150 cm^{-1} (sh, 250 $M^{-1}cm^{-1}$) and 15,110 cm^{-1} (sh, 279 $M^{-1}cm^{-1}$). The low energy band at 18,900 cm^{-1} is assigned as MLCT, while the low energy band at 15,150 cm^{-1} for **1b** is assigned as a $d_{x^2-y^2} \rightarrow d_{xz/yz}$. High energy charge transfer bands (> 30,000 cm^{-1}) are assigned as ligand-based π to π^* transitions for both complexes. Complexes **1b** and **2b** exhibit a ligand-based charge transfer band at ~31,000 cm^{1} that is both more intense and ~3,000 cm^{-1} lower in energy than the lowest energy ligand-based charge transfer band observed for Cu(I) complexes. The decrease in energy is a product of the square planar geometry for the Cu(II) complexes. A square planar conformation is favorable for LLCT processes because inter-ligand donor and acceptor are coplanar to one another.

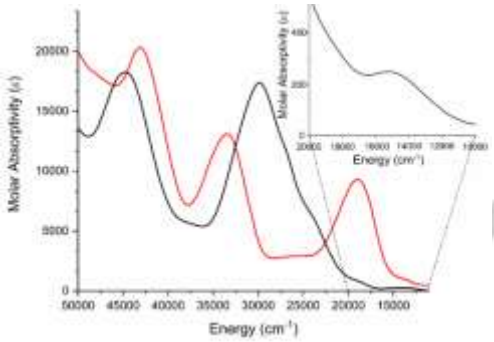

Figure 6. Electronic spectra of **1a** (red) and **1b** (black) in acetonitrile at 25° C. The low intensity band of **1b** is shown in the inset.

Table 6. Electronic spectral data (band maxima) for **1a, 1b, 2a,** and **2b** in acetonitrile

Complex	Energy cm^{-1} (ε, $M^{-1}cm^{-1}$)		
1a	18,900 (9300)	33,330 (13,900)	43,420 (20,190)
1b	15,150 (250)	30,210 (17,040)	45,250 (17,940)
2a	18,870 (10,000)	33,330 (13,240)	44,740 (21,930)
2b	15,110 (279)	31,760 (20,790)	46,930 (26,510)

Computational analysis

Semi-empirical PM3 single point energy calculations were performed for various orientations of the isopropyl substituents (Figure S7) Density functional theory (DFT) calculations were used to better understand the electronic structures of **1a** and **1b** using the B3LYP exchange-correlation functional and 6-31+G** /LANL2DZ basis sets for heavy and light atoms, respectively. Shapes and energy diagrams of the MOs are shown in Figures 7 and 8. The energy differences between the HOMO and LUMO α and β sets for **1b** are greater than those for **1a** by 0.35 eV and 0.08 eV, respectively. The LUMO+2 of **1a** and **1b** α-set are isolated from other virtual orbitals by 2.01 eV and 2.11 eV respectively. LUMO of the β-set is also isolated from other unoccupied orbitals by 0.89 eV.

Population analyses of molecular orbital compositions are given in Table 7. The HOMO for **1a** is comprised largely of copper orbitals (~39%) while the LUMO is mostly ligand in character (~87%). Atomic contributions to the LUMO of **1a** are delocalized across the conjugated system of the dithione ligand. Population analysis and MO diagrams of **1a** and **1b** show equal electron distribution between dithione ligands. Population analysis of the HOMO and LUMO for **1b** show the frontier orbitals to be predominantly ligand in character (~60-90%). The **1b** α-set HOMO is comprised mostly of sulfur orbitals (~70%), whereas the LUMO contributions are distributed like that of **1a**.

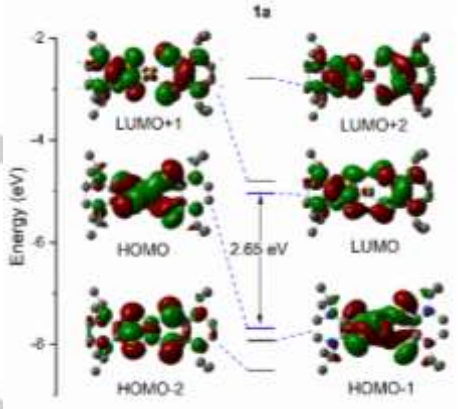

Figure 7. Molecular orbitals and orbital digram for **1a** (isovalue = 0.020).

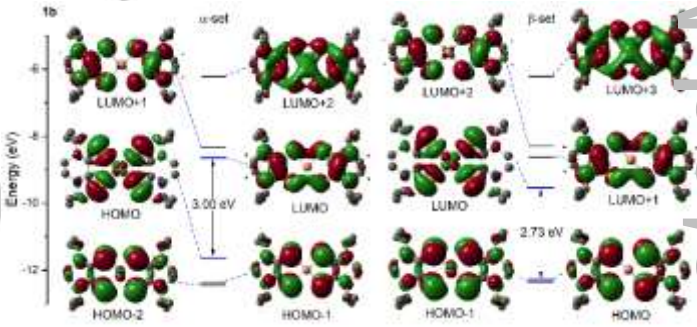

Figure 8. Molecular orbitals and orbital digram for **1b** (isovalue = 0.020)

Table 7. Atomic orbital composition of **1a** and **1b.**

% Composition **1a**

Orbital	E, eV	Cu	Cu (d)	S	N	NCS[a]
LUMO+2	-2.786	1.92	0.39	16.04	19.15	42.34
LUMO+1	-4.793	2.31	1.97	30.51	22.50	43.05
LUMO	**-5.037**	**1.40**	**0.76**	**25.52**	**25.95**	**43.50**
HOMO	**-7.686**	**39.09**	**33.86**	**42.78**	**9.78**	**28.50**
HOMO-1	-7.931	39.98	34.21	44.06	3.74	27.92
HOMO-2	-8.504	35.13	37.87	46.25	11.25	30.18

% Composition **1b** α-set

Orbital	E, eV	Cu	Cu (d)	S	N	NCS[a]
LUMO+2	-6.115	3.68	0.25	19.00	20.12	43.83
LUMO+1	-8.229	0.53	0.52	26.86	28.31	44.66
LUMO	**-8.549**	**1.57**	**0.00**	**16.78**	**34.25**	**44.08**
HOMO	**-11.553**	**14.74**	**14.13**	**69.71**	**5.38**	**30.58**
HOMO-1	-12.249	0.06	0.00	70.93	19.30	46.18
HOMO-2	-12.344	5.20	4.94	67.43	18.32	43.68

% Composition **1b** β-set

Orbital	E, eV	Cu	Cu (d)	S	N	NCS[a]
LUMO+2	-6.104	3.44	0.27	18.68	20.25	43.88
LUMO+1	-8.188	1.49	1.38	25.59	26.67	44.28
LUMO	-8.541	1.65	0.00	17.07	31.02	44.05
HOMO	**-9.436**	**31.20**	**28.47**	**52.30**	**5.65**	**32.41**
HOMO-1	**-12.175**	**0.12**	**0.00**	**71.69**	**18.53**	**46.35**
HOMO-2	-12.258	6.21	5.82	67.35	17.64	43.40

[a] NCS represents the redox active thioamide moiety of the ligands shown Figure S9.

Polarizable continuum model (PCM) TD-DFT calculations of the excited state transitions for complex **1a** are in good agreement with experimental spectra as shown in Figure 10. Modeling the excited state transitions of square planar d^9 copper complexes continues to be a challenge, as complexes containing paramagnetic copper are sensitive to hybrid functionals. [32]

TD-DFT calculations provide a basis for the assignment of experimentally observed bands whose electron transfer can be visualized with electron density difference maps (EDDMs) shown in Figure 11. A model calculation of the excited state geometry for **1a** was performed using an excite state geometry optimization. Optimization of the excited state for the MLCT of **1a** exhibits further distortion of the tetrahedral geometry as shown in Figure 11. The Cu(I) center flattens significantly, with the dihedral angle of the SMS planes changing from 71.88° to 19.80°. One ligand shows a shortening of the dithione C-C bond by 0.09Å, while the other remains unchanged. Optimized geometries and TD-DFT excited state transitions for all calculations are provided in the supporting material Table S5 – S7.

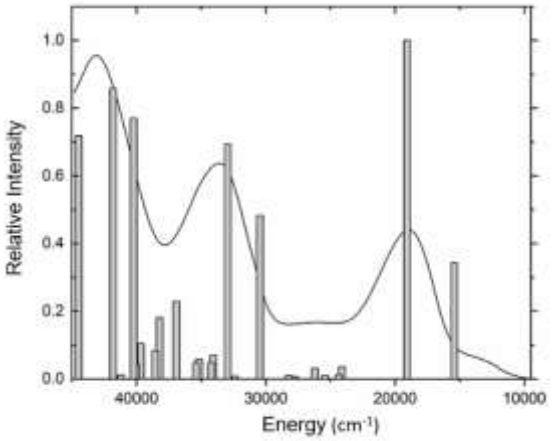

Figure 9. Expeirmental UV-Vis data for **1a** with calculated transitions (grey bars) superimposed. Intensity for both experimental and calculated data are normalized to their maximal values.

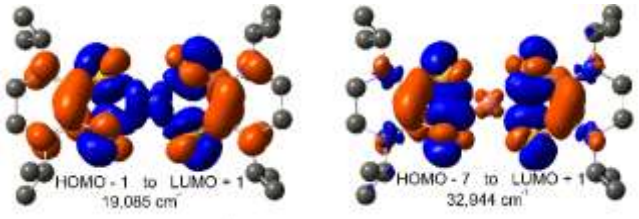

Figure 10. EDDMs for complexes **1a**. Participating molecular orbitals and their energies are listed below each map. Blue orbitals are electron donating orbitals and red orbitals are electron accepting orbitals. A MMLL'CT is shown on the left and a LLCT is shown on the right.

Figure 11. Geometry optimization of the **1a** MLCT (middle) in comparison with the tetrahedral (left) and square planar geometries (right) of **1a** and **1b**.

The population analysis for **1a** and **1b** show that both ligands contribute equally to the molecular orbitals. Virtual orbitals show more participation by the π* orbitals of the dithiolene system, suggesting that the dithione ligand acts as an electron acceptor upon excitation. High extinction coefficients for the low energy bands in the electronic spectra of **1a** and **2a** suggest significant orbital mixing between the copper and sulfur atoms. The absence of such a band for **1b** and **2b** indicates that no such covalency is present for these complexes and the copper ion remains uninvolved in high intensity charge transfer properties.

Molecular orbitals show that the electron distributions of the α and β spin states for **1b** differ in their frontier orbital contribution. The HOMO of the α-set and LUMO of the β-set are mostly sulfur and Cu $d_{x^2-y^2}$ in character. Both the LUMO of the α-set and the LUMO+1 of the β-set are largely dithiolene in character and are very nearly degenerate to one another. The similarity in energy and electron distribution between the two orbitals results in equal likelihood for the ligand-based charge transfers to occur in the α or β spin set.

With the aid of TDDFT, the electronic transitions for **1a** can better understood. The low energy absorption band for **1a** is attributed to a MMLL'CT at ~19,000 cm^{-1}. This band is dominated by a HOMO-1 (34% Cu d_{yz}) to LUMO+1(~95% dithione) transition, which corresponds to a Cu $d_{yz} \rightarrow \pi^*$ transition and ligand-based transition between orthogonal sulfur p-orbitals. During this transition an electron from the copper ion is excited to reduce the accepting dithione ligand. The higher energy region is dominated by LLCTs, which correspond to two bands between 45,000 – 30,000 cm^{-1}. Higher energy transitions are attributed to electronic transfers from out-of-plane sulfur π orbitals to the π^* orbitals in-plane with the dithiolene moiety (participating molecular orbitals for high energy LLCT are given in Table S8).The EDDMs for both the MMLL'CT and LLCT model that the delocalized system of the dithione ligand acts as the electron acceptor. The electron deficient nature of the dithione ligand make them a potent electron accepting moiety in charge transfer processes.

The excited state geometry optimization changes the bond lengths of only one ligand. The effected ligand has shortened conjugated C-C bonds that are more characteristic of the dithiolene ligands, indicating that the ligand is being reduced by accepting electron density from the metal. The change in C-C bond lengths for the acceptor ligand results in a loss of equivalency between the homoleptic ligands, which is apparent in the MOs of the excited state optimization shown in Figure S10.

The distortion from the excited state geometry optimization performed on **1a** produced values of τ_4 = 0.20 and τ_δ = 0.19, indicating a distorted square planar geometry. The ~0.4 decrease in both τ values support that copper donates enough electron density to produce a flattened geometry, resembling that of **1c**. The ability for these complexes to change geometry with changing oxidation state may provide insight into their complicated electrochemical results. As mentioned, these compounds do not exhibit the expected four clearly reversible ligand-based couples. The quasi-reversible ligand-based couples may be due to a geometric arrangement that is occurring as the complex changes in oxidation state. In situ interconversion between copper oxidation states and regeneration of the Cu(II) species is still being investigated.

Conclusions

A new set of Cu(I) and Cu(II) complexes containing fully oxidized dithiolene ligands has been synthesized and characterized by spectroscopic methods, and in representative cases the molecular structures have been determined. The Cu(I) complexes exhibit a metal to ligand low energy charge transfer, while Cu(II) complexes show high energy, ligand to ligand electronic transitions. All complexes exhibit metal-based and partial ligand-based redox couples. The quasi-reversible nature of the ligand couples may be due to changes in the geometry of the complexes. Isopropyl complexes demonstrated less efficient packing due to the lower order of symmetry present in their ligand substituents. Changes in the geometry of the primary coordination sphere dictates copper-sulfur orbital covalency, thus dictating what moiety participates as the electron donor.

Experimental Section

Solvents were purchased from either VWR or Fisher scientific and purified as follows: acetonitrile (MeCN), methylene chloride (CH_2Cl_2), diethyl ether, tetrahydrofuran (THF), dimethyl formamide (DMF), hexane, and toluene, were dried using an LC Technology Solutions Inc., purification system; chloroform ($CHCl_3$) and anhydrous methanol were distilled from CaH_2. $CuCl_2.6H_2O$ was purchased from Aldrich and used as received. $Cu(MeCN)_4ClO_4$ was synthesized using literature procedures.[33] The ligands, N,N-dimethyl piperazine 2,3-dithione (Me_2Dt^0) and N,N-diisopropyl piperazine 2,3-dithione ($^iPr_2Dt^0$) were synthesized in air according to literature procedures.[34] All presented complexes were synthesized under an inert atmosphere using either Schlenk techniques or in a dry box.

All ^1H and ^{13}C NMR spectra were recorded on Bruker 500 or 400 MHz spectrometers. The FTIR spectra of all samples were recorded on a Thermo Scientific Nicolet iS10 spectrometer as neat samples. Elemental analysis was performed at Midwest Microlab LLC., Indianapolis, IN. Electrochemical measurements were carried out using a Metrohm Autolab PGSTAT204 electrochemical analyzer. Voltammograms were recorded at 25ºC with a standard three-electrode system consisting of a platinum working electrode, an Ag^+/Ag reference electrode, and a Pt-wire auxiliary electrode. All voltammograms were internally referenced against the ferrocenium/ferrocene couple. Tetrabutylammonium hexaflourophosphate was used as the supporting electrolyte. Mass spectra was collected via direct injection of MeCN solutions of complexes into the detector of an Agilent 6520 Accurate-Mass Q-TOF LC/MS system to obtain high resolution spectral data.

PM3 semi-empirical calculations were performed *Spartan Student Edition V7* software[35] running on Windows10. DFT calculations were performed using B3LYP functional with 6-31+G**/LANL2DZ basis set with *Gaussian09* software[36] running on Linux OS. Population analysis was calculated using *QMForge* software[37] programs and EDDM's were generated using the *cubegen* package and molecular orbitals generated using *GaussView5.0.9*.

Synthesis

Synthesis of $[Cu(^iPr_2Dt^0)_2][PF_6]$ (**1a**). Into a Schlenk flask, $Cu(MeCN)_4ClO_4$ (0.044 g 0.134 mmol) was dissolved in 50 mL methanol and stirred for 10 minutes before the addition of N,N'-diisopropyl piperazine-2,3-dithione ($^iPr_2Dt^0$) (0.10 g, 0.434 mmol) in 5 mL of chloroform. Upon addition of the ligand, the clear solution turned brown. The reaction mixture was stirred for an hour and during this time the brown mixture turned purple and upon addition of sodium hexafluorophosphate (0.093 g, 0.555 mmol), a green precipitate was formed. Stirring was continued for another 30 minutes before the reaction mixture was filtered and the green product washed with methylene chloride to remove excess ligand and small amounts of methanol (<1 mL) to remove excess $NaPF_6$ to obtain analytically pure product. Yield: 0.093 g (0.138 mmol, 32%). Anal. Calcd (expt.) for $C_{20}H_{36}CuF_6N_4PS_4$: C, 35.89 (35.84); H, 5.42 (5.36); N, 8.37 (8.29); ^1H NMR (CD_3CN): δ 5.31(m, CH, 4H), 3.65(s, CH_2, 8H), 1.34(d, CH_3, 12H), 1.32(d, CH_3, 12H); ^{13}C NMR (CD_3CN): δ 17.37 (CH_3), 41.33 (CH_2), 57.74 (CH), 183.12 (C=S); FTIR (neat, cm^{-1}): 1,587 (vs, C-N), 1,348 (vs, C=S), 829, 596, 555 (vs, PF_6). Electronic spectrum, λ_{max} (nm) in CH_3CN (ε, $M^{-1}cm^{-1}$): 530 (9,300), 377 (2,900), 300 (13,900), 230 (20,190), conductivity, Λ_M = 166 S cm^2 M^{-1}. M^+ Calcd. (Exp) 523.1119 (523.1010)

Synthesis of $[Cu(^iPr_2Dt^0)_2][PF_6]_2$ (**1b**). $Cu(II)Cl_2.2H_2O$ (0.08 g, 0.469 mmol) was dissolved in THF. Two equivalents of the $^iPr_2Dt^0$ ligand (0.22 g, 0.950 mmol) were added and the blue reaction mixture turned green. Upon addition of sodium hexafluorophosphate (0.195 g, 0.950 mmol a dark green precipitate was formed. The precipitate was filtered to obtain an analytically pure product, Yield: 0.360 g (0.442 mmol, 94%). Anal. Calcd. (Expt.) for $C_{20}H_{36}CuF_{12}N_4P_2S_4$: C, 29.50(30.98); H,

4.46(4.95); N, 6.88(7.17); IR (neat, cm^{-1}) : 1,523 (vs, C-N), 1,364 (vs, C=S), 837, 596, 555 (vs, PF_6). Electronic spectrum, λ_{max} (nm) in CH_3CN (ε, $M^{-1}cm^{-1}$): 660 (sh, 250), 331 (17,040), 221 (17,940); conductivity, Λ_M = 240 S cm^2 M^{-1}. M^{2+} Calcd. (Exp) 261.5560 (261.5503)

Synthesis of $[Cu(^iPr_2Dt^0)_2][BF_4]_2$(**1c**). $Cu(II)Cl_2.2H_2O$ (0.04 g, 0.235 mmol) of was dissolved in acetonitrile and stirred for approximately 10 minutes before adding two equivalents of the $^iPr_2Dt^0$ ligand (0.10 g, 0.434 mmol). The blue reaction mixture turned greenish upon addition of sodium tetrafluoroborate (0.047 g, 0.434 mmol). The precipitate was filtered and washed with methylene chloride to remove excess ligand to obtain analytically pure product. Yield: 0.130 g (0.186 mmol, 79%). Anal. Calcd. (Expt.) for $C_{20}H_{36}CuF_8N_4B_2S_4$: C, 34.42 (31.41); H, 5.20 (4.68); N, 8.03(7.13); IR (neat, cm^{-1}): 1,528 (vs, C-N), 1,364 (vs, C=S), 1,025, 1,111 (vs, BF_4).

Synthesis of $[Cu(Me_2Dt^0)_2][PF_6]$ (**2a**). Compound **2a** was synthesized as for **1a** above using Me_2Dt^0 as the ligand. Yield: 0.092 g (0.165 mmol, 48%). Anal. Calcd. (Expt.) for $C_{12}H_{20}CuF_6N_4PS_4$: C, 25.87 (25.79); H, 3.62 (3.62); N, 10.06 (9.75); IR (neat, cm^{-1}) : 1,552 (vs, C-N), 1,364 (vs, C=S), 821, 555, 539 (vs, PF_6). ^1H NMR (400 MHz, CD_3CN): δ 3.86 (s, 8H), 3.58 (s, CH_3, 12H); ^{13}C NMR; δ 46.43 (CH_3), 48.98 (CH_2), 182.35 (C=S). Electronic spectrum, λ_{max} (nm) in CH_3CN (ε, $M^{-1}cm^{-1}$): 530 (10,000), 377 (2,950), 300 (13,240), 227 (21,930) Λ_M = 38.9 S cm^2 M^{-1}. M^+ Calcd. (Exp) 410.9867 (410.9805)

Synthesis of $[Cu(Me_2Dt^0)_2][PF_6]_2$ (**2b**). Compound **2b** was also synthesized as for **1b** above using Me_2Dt^0 as the ligand. Yield: 0.643 g (0.917 mmol, 62%. Anal. Calcd. (Expt.) for $C_{12}H_{20}CuF_{12}N_4P_2S_4$: C, 20.53(21.11); H, 2.87(2.86); N, 7.98(8.14); FTIR (neat, cm^{-1}) : 1552 (vs, C-N), 1364 (vs, C=S), 821, 555, 539 (vs, PF_6). Electronic spectrum, λ_{max} (nm) in CH_3CN (ε,$M^{-1}cm^{-1}$): 662 (279), 314 (20,790) 213 (26,510), Λ_M = 238 S cm^2 M^{-1}. M^{2+} Calcd. (Exp) 205.4934 (205.4981)

Molecular structure determination

High quality single crystals of **1a**, **2a**, and **1c** were grown by slow diffusion of ether into an acetonitrile solution of the complexes. The crystals were selected, coated with paratone oil, mounted on a glass fiber, and X-ray data were collected using a Bruker SMART Apex II diffractometer with a graphite monochromator for Mo K_α radiation (0.71073 Å). Data was collected at 296 K. The absorption correction was performed using the SADABS[38] routine. The structures were solved using SHELXS-97[39] and SHEXLX-2018[40]. All non-hydrogen atoms were refined anisotropically. Hydrogen atoms were placed at calculated positions and refined as riding atoms with isotropic displacement parameters.

Crystals of **2a** were non-merohedrally twinned. The orientation matrices for the two components were identified using the Cell Now, with the two components being related by a 180° rotation around the reciprocal axis (0 1 0). The two components were integrated using Saint, resulting in a total of 20,780 reflections. 4,070 reflections (2,266 unique) involved component 1 only (mean I/sigma = 36.4), 4,015 reflections (2,232 unique) involved component 2 only (mean I/sigma = 23.8), and 13,032 reflections (5,809 unique) involved both components (mean I/sigma = 31.5). The exact twin matrix identified by the integration program was found to be -0.99992 0.00057 -0.00017, 0.51527 0.99993 0.10994, 0.00038-0.00135 -1.00001. The data were corrected for absorption using twinabs, and the structure was solved by direct methods with only the non-overlapping reflections of component 1. The structure was refined using the hklf 5 routine with all reflections of component 1 (including the overlapping ones), resulting in a BASF value of 0.293(1).

The tetrafluoro borate anion of crystal **1c** was refined as disordered over two moieties with different rotational orientations. The two moieties were restrained to have close to tetrahedral geometry and to be similar to each other. U_{ij} components of atomic displacement parameters (ADPs) of disordered atoms were restrained to be similar. Subject to these conditions, the occupancy ratio refined to 0.643(7) to 0.357(7). Crystals of **1c** contained an acetonitrile solvent molecule. The acetonitrile molecule is 1:1 disordered around a twofold axis, with the middle carbon atom located essentially on this axis. Correlation between the two symmetry equivalent copies of this atom created an unstable refinement and slightly unreasonable atom positions. To overcome these problems the atom was restrained to lie close to the special position on the two-fold axis by restraining the distances of the atom to the methyl C and N atom to be each close to that of their symmetry created counterparts. U_{ij} components of ADPs of disordered atoms were restrained to be similar.

Acknowledgements

J.B. acknowledges The Air Force Office of Scientific Research (AFOSR) LRIR #18RQCOR100, and the Aerospace Systems Directorate (AFRL/RQ). This research was performed while the J.B. held an NRC Research Associateship award at the Air Force Research Laboratory. We would also like to acknowledge Dr. Jingzhi Pu, IUPUI for helpful discussions. This research was supported in part by Lilly Endowment, Inc., through its support for Indiana University Pervasive Technology Institute, and in part by the Indiana METACyt Initiative. The Indiana MTACyt Initiative at IU was also supported in part by Lilly Endowment, Inc.

Keywords: Copper • Redox active ligand • Charge transfer • Dithione • Oxidation dependent charge transfer.

References

WILEY-VCH

FULL PAPER

Entry for the Table of Contents

Layout 1:

FULL PAPER

Copper complexes of oxidized dithione ligands have been synthesized and characterized. The complexes exhibit intense charge transfer transitions depending on the oxidation state of copper.

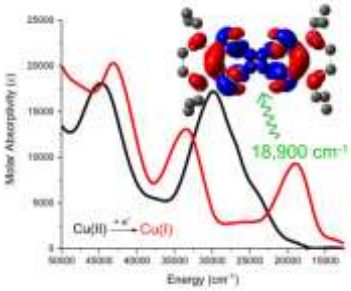

*Kyle J. Colston,Dr. Sara A. Dille, Dr. Benjamin Mogesa, Dr. Andrei V. Astashkin, Dr. Jacilynn A. Brant, Dr. Matthias Zeller, and Dr. Partha Basu**

Key topic: redox active ligand, charge transfer.

[1] C. K. Jorgensen, *Coord. Chem. Rev.* **1966**, *1*, 164-178.
[2] V. Balzani, G. Bergamini, S. Campagna and F. Puntoriero in *Photochemistry and Photophysics of Coordination Compounds: Overview and General Concepts*, Eds.: V. Balzani and S. Campagna), Springer Berlin Heidelberg, **2007**, pp. 1-36.
[3] a) L. Pilia, D. Espa, A. Barsella, A. Fort, C. Makedonas, L. Marchio, M. L. Mercuri, A. Serpe, C. A. Mitsopoulou and P. Deplano, *Inorg. Chem.* **2011**, *50*, 10015-10027; b) S. D. Cummings, L.-T. Cheng and R. Eisenberg, *Chem. Mater.* **1997**, *9*, 440-450.
[4] a) B. Zhou, Y. Idobata, A. Kobayashi, H. Cui, R. Kato, R. Takagi, K. Miyagawa, K. Kanoda and H. Kobayashi, *J. Am. Chem. Soc.* **2012**, *134*, 12724-12731; b) Y. Sun, S. Peng, C. Di, F. Jiao, W. Xu, D. Qiu and D. Zhu, *Adv. Mater.* **2012**, *24*, 932-937; c) Y. Idobata, B. Zhou, A. Kobayashi and H. Kobayashi, *J. Am. Chem. Soc.* **2012**, *134*, 871-874; d) F. Schoedel, U. Tutsch, F. Isselbaecher, D. Schweitzer, I. Saenger, M. Bolte, J. W. Bats, J. Mueller, M. Lang, M. Wagner and H.-W. Lerner, *Eur. J. Inorg. Chem.* **2011**, 1205-1211; e) B. Zhou, H. Yajima, A. Kobayashi, Y. Okano, H. Tanaka, T. Kumashiro, E. Nishibori, H. Sawa and H. Kobayashi, *Inorg. Chem.* **2010**, *49*, 6740-6747; f) Y. Wang, L. Ren, Y. Shen, Z. Li, Z. Peng and B. Yuan, *Acta Chim. Sinica* **2009**, *67*, 1469-1474; g) X. Wang, *Chemistry and Bioengineering* **2006**, *23*, 15-17; h) G. Kochurani, K. Kandasamy, H. B. Singh and B. Varghese, *Indian J. Chem., Sect. A: Inorg., Bio-inorg., Phys., Theor. Anal. Chem.* **2003**, *42A*, 2344-2351; i) X. Chi, J. Yan and X. Li, *Chinese J. Syn. Chem.* **2003**, *11*, 142-146; j) Q. Zhu, J. Dai, G. Bian, X. Wang, W. Yang and Z. Yan, *Synth. React. Inorg. Met.-Org. Chem.* **2002**, *32*, 1001-1012; k) H. Tanaka, H. Kobayashi and A. Kobayashi, *J. Am. Chem. Soc.* **2002**, *124*, 10002-10003; l) Y. Misaki, Y. Tani, K. Takahashi and K. Tanaka, *Mol. Cryst. Liq. Cryst. Sci. Technol., Sect. A* **2002**, *379*, 71-76; m) X. Chi and L. Xiao-ping, *Chinese J. Syn. Chem.* **2002**, *10*, 366-369; n) E. Cerrada, M. C. Diaz, C. Diaz, M. Laguna and A. Sabater, *Synth. Met.* **2001**, *119*, 91-92.
[5] V. A. Starodub, S. V. Vitushkina, D. Kamenskyi, A. G. Anders, V. O. Cheranovskii, H. Schmidt, D. Steinborn, I. Potocnak, M. Kajnakova, A. Radvakova and A. Feher, *J. Phys. Chem. Solids* **2012**, *73*, 350-356.
[6] a) U. T. Mueller-Westerhoff, B. Vance and D. I. Yoon, *Tetrahedron* **1991**, *47*, 909-932; b) H. Kisch, *Comments Inorg. Chem.* **1994**, *16*, 113-132; c) W. F. Guo, X. B. Sun, J. Sun, W. T. Yu, X. Q. Wang, G. H. Zhang and D. Xu, *Cryst. Res. Technol.* **2007**, *42*, 522-528; d) X. Q. Wang, Q. Ren, F. J. Zhang, W. F. Guo, X. B. Sun, J. Sun, H. L. Yang, G. H. Zhang, X. Q. Hou and D. Xu, *Mater. Res. Bull.* **2008**, *43*, 2342-2353; e) Y.-L. Wang, D. Xu, W.-T. Yu, X.-B. Sun, Q. Ren, G.-h. Zhang, Y.-Q. Ding, X.-q. Wang, W.-f. Guo, H.-Y.

Chen and L. Feng, *J. Coord. Chem.* **2008**, *61*, 768-775.
[7] a) W. Paw and R. Eisenberg, *Inorg. Chem.* **1996**, *36*, 2287-2293; b) L. A. Cameron, J. W. Ziller and A. F. Heyduk, *Chem. Sci.* **2016**, *7*, 1807-1814; c) W. A. Tarran, G. R. Freeman, L. Mrphy, A. M. Benham, R. Kataky and J. A. G. Williams, *Inorg. Chem.* **2014**, *53*, 5738-5749.
[8] E. A. M. Geary, L. J. Yellowlees, L. A. Jack, L. D. H. Oswald, S. Parsons, N. Hirata, J. R. Durrant and N. Robertson, *Inorg. Chem.* **2005**, *44*, 242-250.
[9] K. Mebrouk, F. Camerel, O. Jeannin, B. Heinrich, B. Donnio and M. Fourmigue, *Inorg. Chem.* **2016**, *55*, 1296-1303.
[10] a) F. A. Devillanova, A. Diaz, F. Isaia, G. Verani, L. P. Battaglia and A. B. Corradi, *J. Coord. Chem.* **1986**, *15*, 161-172; b) F. Bigoli, M. A. Pellinghelli, P. Deplano, E. F. Trogu, A. Sabatini and A. Vacca, *Inorg. Chim. Acta* **1991**, *180*, 201-207; c) F. Bigoli, M. A. Pellinghelli, P. Deplano and E. F. Trogu, *Inorg. Chim. Acta* **1991**, *182*, 33-39.
[11] a) D. Fuhrmann, S. Dietrich and H. Krautscheid, *Chem. Eur. J.* **2017**, *23*, 3338-3346; b) E. Allwright, G. Silber, J. Crain, M. M. Matsushita, K. Awaga and N. Robertson, *Dalton Trans.* **2016**, *46*, 9363-9368; c) S. H. Schlindwein, M. R. Ringerberg, M. Nieger and D. Gudat, *Z. Anorg. Allg. Chem* **2017**, *643*, 1628-1634.
[12] N. Robertson and L. Cronin, *Coord. Chem. Rev.* **2002**, *227*, 93-127.
[13] a) Y. Yokoyama, S. Suzuki, H. Furihata, S. Takahi, M. Nomura and M. Kajitan, *Synthesis* **2004**, 701-705; b) M. Vedichi and S. K. Das, *Inorg Chem.* **2006**, *45*, 10037-10039; c) S. S. Attar, L. Marchio, L. Pilia, M. F. Casula, D. Espa, A. Serpe, M. Pizzotti, D. Marinotto and P. Deplano, *New J. Chem.* **2019**, *43*, 12570-12579.
[14] F. A. Cotton, G. Wilkinson, M. Bochmann and C. Murillo, *Advanced Inorganic Chemistry, 6th Edition*, Wiley, **1998**, p. 1248 pp.
[15] a) B. Mogesa, E. Perera, H. M. Rhoda, J. K. Gibson, J. Oomens, G. Berden, M. J. v. Stipdonk, V. N. Nemykin and P. Basu, *Inorg. Chem.* **2015**, *54*, 7703-7716; b) S. C. Ratvasky, B. Mogesa, M. J. v. Stipdonk and P. Basu, *Polyhedron* **2016**, *114*, 370-377; c) E. Perera and P. Basu, *Dalton Trans.* **2009**, 5023-5028; d) R. P. Mtei, E. Perera, B. Mogesa, B. Stein, P. Basu and M. L. Kirk, *Eur. J. Inorg. Chem.* **2011**, *2011*, 5467-5470; e) V. N. Nemykin, J. G. Olsen, E. Perera and P. Basu, *Inorg. Chem.* **2006**, *45*, 3557-3568.
[16] W. J. Geary, *Coord. Chem. Rev.* **1971**, *7*, 81-122.
[17] L. Antolini, A. C. Fabretti, G. Franchini, L. Menabue, G. C. Pellacani, H. O. Desseyn, R. Dommisse and H. C. Hofmans, *Dalton Trans.* **1987**, 1921-1928.
[18] CCDC in *Structural search for all [CuII/I(Dt)23-/2- complexes, Vol.* Cambridge Crystallographic Database, **2018**.
[19] a) W. Levason, M. Nirwan, R. Ratnani, G. Reid, N. Tsoureasa and M. Webstera, *Dalton Trans.* **2007**, 439–448; b) W. K. Musker, M. M. Olmstead and R. M. Kessler, *Inorg. Chem.* **1984**, *23*, 3266-3269; c) L. L. Diaddrio, E. R. Dockal, M. D. Glick, L. A. Ochrymowycz and D. B. Rorabacher, *Inorg Chem* **1985**, *24*, 356-363; d) M. M. Olmstead, W. K. Musker and R. M. Kessler, *Inorg. Chem.* **1981**, *20* 151-157.
[20] L. B. Colin in *Structures and Structural Trends in Homoleptic Dithiolene Complexes*, *Vol. 52* (Ed. K. D. Karlin), John Wiley and Sons Inc., Iselin, NJ, **2004**, p. 2.
[21] C. L. Beswick, J. M. Schulman and E. I. Stiefel, *Prog. Inorg. Chem.* **2003**, *52*, 55-110.
[22] L. Yang, D. R. Powell and R. P. Houser, *Dalton Trans.* **2007**, 955-964.
[23] M. H. Reineke, M. D. Sampson, A. L. Rheingold and C. P. Kubiak, *Inorg. Chem.* **2015**, *54*, 3211-3217.
[24] J. D. Forrester, A. Zalkin and D. H. Templeton, *Inorg. Chem.* **1964**, *3*, 1507-1515.
[25] X. M. Ren, G. X. Liu, H. Xu, T. Akutagawa and T. Nakamura, *Polyhedron* **2009**, *28*, 2075-2079.
[26] V. Madhu and S. K. Das, *Polyhedron* **2004**, *23*, 1235-1242.
[27] CCDC in *Cambridge Crystallographic Data Centre, Vol.* Cambridge, **2019**.
[28] G. A. Bain and J. F. Berry, *J. Chem. Educ.* **2008**, *85*, 532-536.
[29] J. Peisach and W. E. Blumberg, *Arch. Biochem. Biophys.* **1974**, *165*, 69-708.

[30] G. C. Pellacani, G. Peyronel and A. Pignedoli, *Gazz. Chim. Ital.* **1972**, *102*, 835-846.
[31] P. Basu, *J. Chem. Educ.* **2001**, *78*, 666-669.
[32] a) A. M. Whyte, B. Roach, D. K. Henderson, P. A. Tasker, M. M. Matsushita, K. Awaga, F. J. White, P. Richardson and N. Robertson, *Inorg. Chem.* **2011**, *50*, 12867-12876; b) N. Marom and L. Kronik, *Appl. Phys. A: Mater. Sci. Process.* **2009**, *95*, 159-163; c) N. Marom, O. Hod, G. E. Scuseria and L. Kronik, *J. Chem. Phys.* **2008**, *128*, 164107/164101-164107/164106.
[33] P. C. I. Kierkegaard and R. Norrestam, *Acta Cryst.* **1975** *314*, 314-315.
[34] R. Isaksson, T. Liljefors and J. Sandstroem, *J. Chem. Res., Synop.* **1981**, 43.
[35] in *Spartan Student Edition*, *Vol.* Wavefunction Inc., www.wavefun.com, **2014**.
[36] G. W. T. M. J. Frisch, H. B. Schlegel, G. E. Scuseria, M. A. Robb, J. R. Cheeseman, G. Scalmani, V. Barone, G. A. Petersson, H. Nakatsuji, X. Li, M. Caricato, A. Marenich, J. Bloino, B. G. Janesko, R. Gomperts, B. Mennucci, H. P. Hratchian, J. V. Ortiz, A. F. Izmaylov, J. L. Sonnenberg, D. Williams-Young, F. Ding, F. Lipparini, F. Egidi, J. Goings, B. Peng, A. Petrone, T. Henderson, D. Ranasinghe, V. G. Zakrzewski, J. Gao, N. Rega, G. Zheng, W. Liang, M. Hada, M. Ehara, K. Toyota, R. Fukuda, J. Hasegawa, M. Ishida, T. Nakajima, Y. Honda, O. Kitao, H. Nakai, T. Vreven, K. Throssell, J. A. Montgomery, Jr., J. E. Peralta, F. Ogliaro, M. Bearpark, J. J. Heyd, E. Brothers, K. N. Kudin, V. N. Staroverov, T. Keith, R. Kobayashi, J. Normand, K. Raghavachari, A. Rendell, J. C. Burant, S. S. Iyengar, J. Tomasi, M. Cossi, J. M. Millam, M. Klene, C. Adamo, R. Cammi, J. W. Ochterski, R. L. Martin, K. Morokuma, O. Farkas, J. B. Foresman, and D. J. Fox in *Gaussian 09, Vol.* **2009**.
[37] A. Tenderhold in *QMForge 2.4*, *Vol.* http://qmforge.sourceforge.net.
[38] G. M. Sheldrick, *University of Göttingen,Germany* **2002**.
[39] G. M. Sheldrick, *Acta Crystallogr., Sect. A: Found. Crystallogr.* **2008**, *64*, 112-122.
[40] G. M. Sheldrick, *Acta Crystallogr., Sect. A: Found. Adv.* **2015**, *71*, 3-8.